Strong bulk plasma acceleration in Earth's magnetosheath: A magnetic slingshot effect?

B. Lavraud,[1] J. E. Borovsky,[1] A. J. Ridley,[2] E. W. Pogue,[1] M. F. Thomsen,[1] H. Rème,[3] A. N. Fazakerley,[4] and E. A. Lucek[5]

Received 14 March 2007; revised 27 April 2007; accepted 15 May 2007; published 18 July 2007.

[1] In the near-Earth environment, strong bulk plasma accelerations are frequently taken to be the diagnostic of the occurrence of magnetic reconnection. In this letter, we report new and unambiguous spacecraft observations and corresponding magnetohydrodynamic (MHD) simulation of strong bulk plasma acceleration in the terrestrial magnetosheath during low Alfvén Mach number solar wind conditions, which is demonstrably not associated with magnetic reconnection. We illustrate this effect with Cluster spacecraft data that show plasma accelerations up to speeds of 1040 km/s, while the ambient solar wind speed is only 650 km/s (i.e., in excess by 60%). Based on a comparison with global MHD simulations of the magnetosphere, we show that the acceleration results from enhanced magnetic forces exerted on the plasma by "stiff" magnetic flux tubes in a low-β magnetosheath that result from the low Alfvén Mach number solar wind. The MHD simulations demonstrate that the acceleration is asymmetric, as well as the magnetopause shape, and is the result of both magnetic pressure gradient and tension forces, showing that this effect is not a simple analogy to a "slingshot effect" for which magnetic tension would dominate. Like magnetic reconnection, this mechanism is capable of producing strong plasma acceleration in the near-Earth's environment. The low Alfvén Mach number solar wind condition leading to this mechanism is often characteristic of coronal mass ejections (CMEs). **Citation:** Lavraud, B., J. E. Borovsky, A. J. Ridley, E. W. Pogue, M. F. Thomsen, H. Rème, A. N. Fazakerley, and E. A. Lucek (2007), Strong bulk plasma acceleration in Earth's magnetosheath: A magnetic slingshot effect?, *Geophys. Res. Lett.*, *34*, L14102, doi:10.1029/2007GL030024.

1. Introduction

[2] The terrestrial magnetic field is an obstacle that causes the solar wind to decelerate and divert at the bow shock, located about 15 Earth radii (R_E) upstream (see Figure 1). The shock heating of the solar-wind plasma gives rise to a hot plasma region downstream from the shock, the magnetosheath, which surrounds the Earth's magnetosphere [*Spreiter et al.*, 1966a, 1966b]. The flowing magnetosheath is the region interacting with the Earth's magnetosphere. This coupling leads to numerous phenomena, of which the occurrence of magnetic reconnection is of prime importance [*Dungey*, 1961; *Paschmann et al.*, 1979; *Sonnerup et al.*, 1981].

[3] At the boundary between the magnetosheath and magnetosphere, the magnetopause, magnetic reconnection leads to strong bulk plasma accelerations as the magnetic stresses resulting from the new magnetic configuration transforms magnetic energy into kinetic energy. The strong bulk plasma accelerations are observed on the Earthward side of the magnetopause [e.g., *Paschmann et al.*, 1979; *Sonnerup et al.*, 1981; *Cowley*, 1982; *Gosling et al.*, 1990a] since it is the plasma entering through the newly open boundary that is subject to magnetic stresses.

[4] Early studies described the flow of the magnetosheath plasma by means of hydrodynamic concepts [*Spreiter et al.*, 1966a, 1966b]. In reality, the flow behavior is affected by magnetic fields. The magnetic forces that act on the flows become larger as the solar wind Alfvén Mach number $M_A = |\boldsymbol{V}|/(|\boldsymbol{B}|(\rho\mu_0)^{-1/2})$ and subsequent magnetosheath thermal $\beta = nk_BT/(\boldsymbol{B}^2/2\mu_0)$ are lower [*Spreiter et al.*, 1966a] (with $\boldsymbol{V}$ the solar wind speed, $\boldsymbol{B}$ the magnetic field magnitude, ρ the plasma mass density, n the number density, T the temperature, k_B the Boltzmann constant, and μ_0 the permeability of free space). Such conditions tend to occur when CMEs pass the Earth [*Gosling et al.*, 1987; *Lindsay et al.*, 1995; *Farrugia et al.*, 1995].

[5] Some effects, like the formation of a plasma depletion layer in the sub-solar region, can even be opposite to the predictions of hydrodynamics, i.e., decrease in density but increase in magnetic field on approach to the sub-solar magnetopause [*Zwan and Wolf*, 1976], and are fundamentally magnetohydrodynamic (MHD) in nature [*Phan et al.*, 1994; *Farrugia et al.*, 1995; *Siscoe et al.*, 2002]. Magnetosheath flows that exceeded that of the solar wind by 10–20 % have early been reported [*Howe and Binsack*, 1972; *Chen et al.*, 1993; *Petrinec et al.*, 1997]. Such observations were first interpreted in terms of enhanced magnetic tension of draped magnetic flux tubes that accelerates magnetosheath plasma along the magnetopause in the fashion of a magnetic "slingshot" [*Chen et al.*, 1993]. However, it was later argued [*Petrinec et al.*, 1997] that such observations may result from either reconnection-related processes or high-energy particle leakage, and that magnetosheath flow may not exceed the solar wind speed by more than a few percent.

2. Cluster Observations

[6] The event analyzed here occurred during the passage of a coronal mass ejection (CME) at Earth on November

[1]Space Science and Applications, Los Alamos National Laboratory, Los Alamos, New Mexico, USA.
[2]Center for Space Environment Modeling, University of Michigan, Ann Arbor, Michigan, USA.
[3]Centre d'Etude Spatiale des Rayonnements, Toulouse, France.
[4]Mullard Space Science Laboratory, University College London, Dorking, UK.
[5]Blackett Laboratory, Imperial College, London, UK.

0094-8276/07/2007GL030024

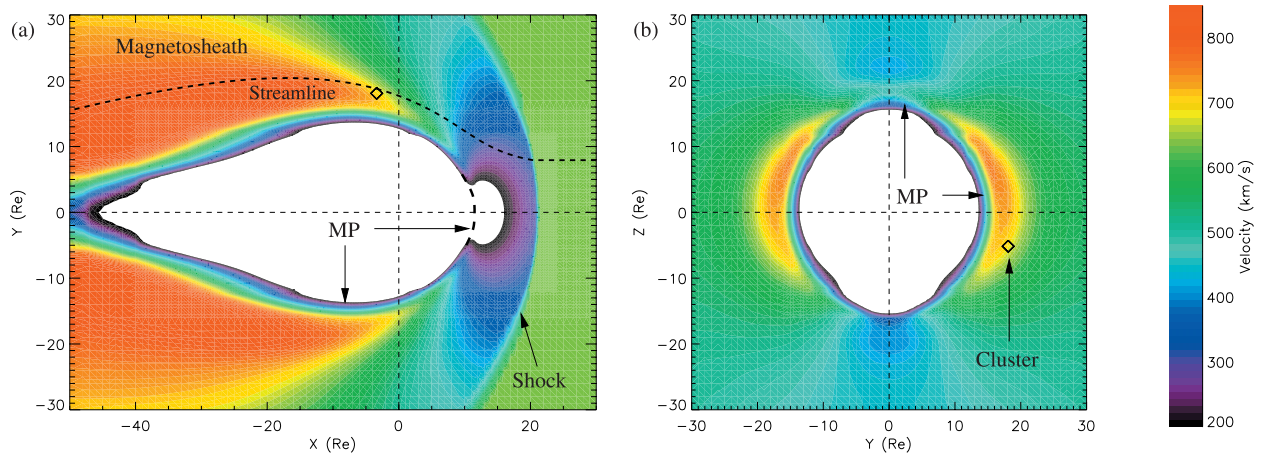

Figure 1. (a) X-Y plane 2D cut of the bulk plasma speed (with same color palette as Figure 1b) after two hours of global MHD simulation for the steady conditions defined as run 1 in the text, i.e., for a low Alfvén Mach number solar wind. A flow streamline passing in the large plasma flow region, and used in section 4, is shown with a black dashed line. The solar wind flows from the Sun (right side) and the bow shock and magnetopause are illustrated. (b) Y-Z plane 2D cut of the plasma speed for the same run at a downtail distance X = −5 R_E. Cluster 1 location (projection) at 9 UT on November 25th 2001, i.e., during similar solar wind conditions, is shown with black diamonds.

25th, 2001. The CME has been identified as a magnetic cloud [*Cane and Richardson*, 2003]. Around 09:00 UT on that day the four Cluster spacecraft were located at (−3.4, 18.0, −5.2) Earth Radii (R_E; GSM coordinates) on the dusk-side southern flank of the magnetosphere near the dawn-dusk terminator (see Figure 1). Figure 2 shows Cluster 1 data and ACE solar wind conditions (lagged by 2400 s) for the interval 09:00 – 09:30 UT. During this interval, the interplanetary magnetic field (IMF) is strongly northward (Figure 2h), the solar wind velocity is about 650 km/s (Figure 2c), and both are steady for several hours outside of the interval shown here. At around 9:15 UT the density (Figure 2g) increases to ∼5 cm^{-3}; this produces a compression of the magnetosphere and Cluster crosses the magnetopause (vertical dashed line in Figure 2) and enters the magnetosheath from the magnetosphere. The Alfvén Mach number (M_A) of the solar wind is low during this interval: M_A = 2.0 before the density jump and 4.4 after, which compares to $M_A \sim 8$ or more for regular solar wind conditions.

[7] Upon entering the magnetosheath, very large flows are observed by the three operating ion instruments onboard the spacecraft, up to 1040 km/s on two of them, while the solar wind speed is only ∼650 km/s (Figure 2c). These flows are mainly perpendicular to the magnetic field (Figure 2d) and the flowing magnetosheath plasma is characterized by a thermal β much lower than unity (Figure 2f), which is expected for low M_A solar wind [*Farrugia et al.*, 1995].

[8] While such large plasma acceleration is often taken to be the signature of magnetic reconnection, several arguments demonstrate that this is not the case here. First, Cluster magnetic field data (Figure 2e) show a clear current sheet discontinuity at 09:12:30 UT, as is typically observed for crossings of the magnetopause current layer. Secondly, this magnetic discontinuity also corresponds to a discontinuity in the energy flux spectrograms of both ions (Figure 2b) and electrons (Figure 2a), with the fluxes of high energy electrons around 1 keV dropping tremendously right at the boundary before the flows are detected. This latter characteristic corresponds to a drop in electron (and ion) temperature. High energy electrons (>1 keV) are extremely fast (much faster than the bulk flow speed). The lack of such electrons in the large flow region demonstrates that this region is not magnetically connected to the magnetosphere (where such electrons are present, as seen before 09:15 UT), and thus that the flows cannot be the result of particle leakage. These observations thus also constitute an unambiguous proof that Cluster is outside the magnetopause when the fast flows are detected [*Gosling et al.*, 1990b; *Fuselier et al.*, 1997; *Lavraud et al.*, 2006]. Because magnetic reconnection leads to enhanced flows inside the magnetopause [*Paschmann et al.*, 1979; *Cowley*, 1982], these flows are not the result of magnetic reconnection.

[9] Because of the solar wind density jump around 09:15 UT, the magnetopause crossing is extremely rapid. Using a multi-spacecraft discontinuity analysis technique [*Dunlop et al.*, 2002], we determine a lower limit for the magnetopause normal speed of ∼400 km/s for this crossing. This result means, although the enhanced flows are largest close to the magnetopause and recorded for a rather short period, that this flow layer extends to some distance away from the magnetopause. This dynamic crossing led the spacecraft to rapidly scan the magnetosheath profile, possibly over more than ten R_E in a few minutes.

3. Global MHD Simulations

[10] BATS-R-US is a 3-D global MHD model of the solar wind-magnetosphere-ionosphere interaction [*Gombosi et al.*, 2000; *Ridley et al.*, 2004]. The model is based on the equations of ideal single-fluid MHD. These equations are solved on a three-dimensional grid wherein the cell size increases away from Earth.

[11] To illustrate the physics of the mechanism that results in large magnetosheath flows, we made two runs of the global MHD model with steady solar wind parameters. Run 1 corresponds to a low M_A (∼2) with solar wind conditions corresponding to those during the interval 09:00 – 09:15 UT with n = 1 cm^{-3}, $|V|$ = 650 km/s and IMF B_Z = 15

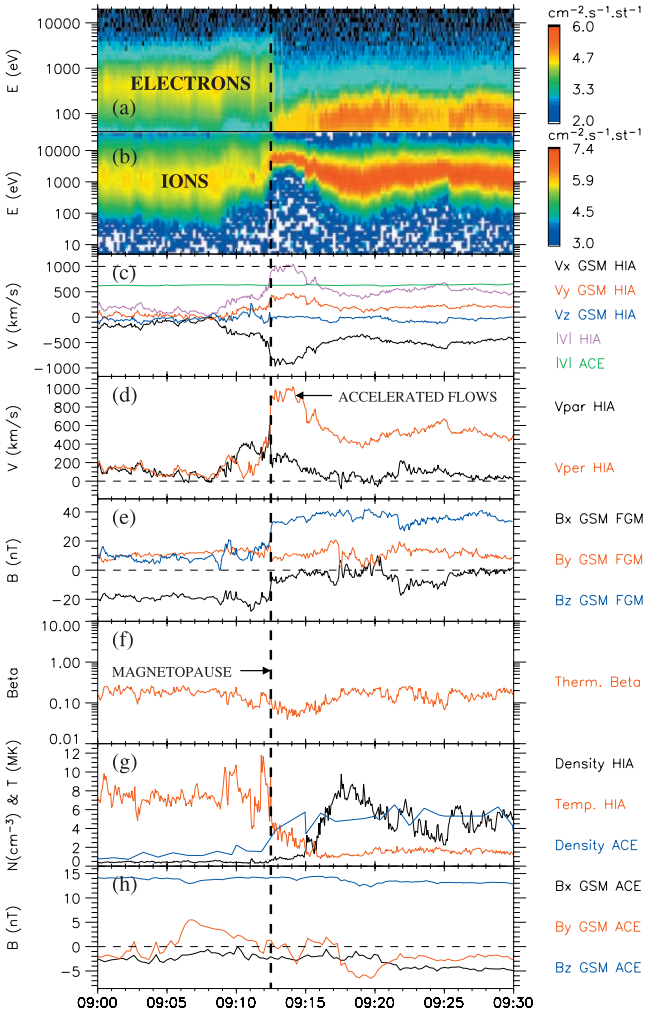

Figure 2. Cluster 1 and ACE data for the magnetopause crossing on November 25th, 2001. The vertical dashed line shows the magnetopause. (a) Cluster omni-directional electron spectrogram. (b) Cluster omni-directional ion spectrogram. (c) Cluster GSM ion velocity components, together with ACE solar wind bulk speed (green). (d) Cluster parallel and perpendicular components of the velocity. (e) Cluster GSM magnetic field components. (f) Cluster thermal β (ratio of thermal to magnetic pressures). (g) Cluster ion density and temperature, together with ACE solar wind density. (h) ACE GSM IMF components. Solar wind data are lagged by 2400 s to account for advection from ACE to the Earth. The magnetosphere is to the left of the magnetopause and the magnetosheath to the right. This crossing shows the occurrence of intense flows outside the magnetopause in the magnetosheath.

nT. Run 2 corresponds to more typical solar wind conditions with $n = 5$ cm^{-3}, $|\boldsymbol{V}| = 650$ km/s and IMF $B_Z = 5$ nT. Figure 1a shows a cut in the equatorial X-Y_{GSM} plane of the bulk speed from run 1, together with the Cluster 1 location at 09:00 UT on November 25th, 2001 for context.

[12] Figure 1a shows two layers of large flows along the flanks of the magnetosphere, to speeds higher than 850 km/s. Such speeds are substantially higher than the input solar wind speed of 650 km/s. Although not shown, the large flow regions in run 1 are characterized by slightly hotter and less dense plasma as compared to the magnetosheath further from the magnetopause. These MHD results are thus compatible with Cluster measurements close to the dusk magnetopause during the interval of November 25th, 2001 when comparable solar wind conditions prevailed. However, it is noted that the flow exceeds that of the solar wind by more than 30% in the simulation while the acceleration observed by Cluster for similar solar wind conditions exceeds that of the solar wind by up to 60%. The reasons for such a quantitative difference will deserve future investigations (see section 5).

[13] Figure 1b shows a cut in the Y-Z_{GSM} plane at $X_{GSM} = -5$ R_E of the plasma speed from run 1. A comparison of Figures 1a and 1b shows that plasma acceleration is asymmetric with the high speeds observed along the dawn and dusk flanks and lower speeds observed over the poles. In addition, the magnetosphere (i.e., magnetopause) appears elongated in the North-South direction. As detailed below, this asymmetry in both the flows and magnetopause shape may be expected since magnetic forces act perpendicular to the magnetic field. Under the prevailing northward IMF, the strongest magnetic forces are expected along the flanks. As the IMF rotates, the location of flow enhancement and the magnetopause elongation follow the rotation so that for more horizontal IMF the large flows are located over the poles of the magnetosphere and the magnetopause is elongated in the dawn-dusk direction. Such cases have been found but are not shown here and left for a more exhaustive study of low Mach number effects on solar wind – magnetosphere coupling (cf. section 5).

4. Interplay Between MHD Forces

[14] To investigate the possible magnetic slingshot nature of this acceleration, we make use of MHD runs 1 and 2 in Figure 3. From each simulation, we have selected a magnetosheath flow streamline that passes in the dusk-flank magnetosheath, such as illustrated in Figure 1a for run 1.

[15] It is first noted that the bow shock, indicated in both cases by a sharp deceleration (Figures 3a and 3d), is located further from the Earth in the low M_A case although the dynamic pressure is lower for this simulation. As explained by *Russell and Petrinec* [1996], the bow shock intuitively ought to retreat Sunward as the solar wind Mach numbers approach 1 (both Alfvénic (M_A) and magnetosonic (M), with $M_A > M$).

[16] Figure 3 displays the accelerations resulting from the MHD forces at work and the speed profile along the streamlines selected for each run. The acceleration due to each force is simply calculated along the streamlines according to the steady state MHD momentum equation (equation 1).

$$\rho(\boldsymbol{V}\cdot\nabla)\boldsymbol{V} = -\nabla p + \boldsymbol{J}\times\boldsymbol{B} \tag{1}$$

$$\boldsymbol{J}\times\boldsymbol{B} = \frac{1}{\mu_0}(\boldsymbol{B}\cdot\nabla)\boldsymbol{B} - \nabla\left(\frac{\boldsymbol{B}^2}{2\mu_0}\right) \tag{2}$$

$$\frac{\partial \boldsymbol{V}}{\partial \boldsymbol{s}} = \boldsymbol{A}_{\nabla p} + \boldsymbol{A}_{\nabla B} + \boldsymbol{A}_{CurvB} \tag{3}$$

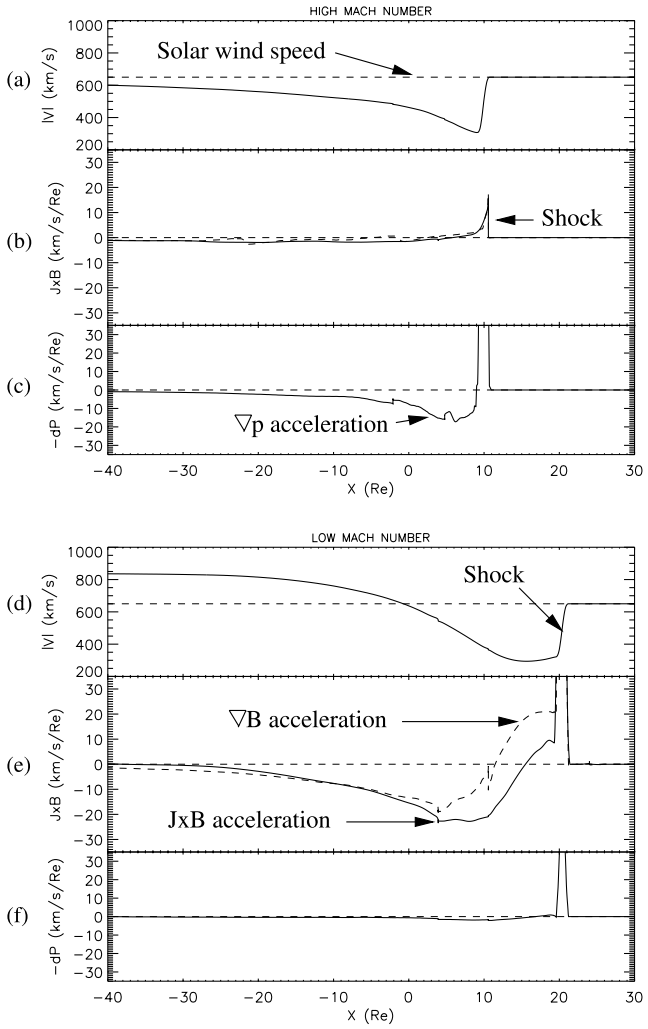

Figure 3. Analysis of global MHD results from the two runs described in the text, i.e., respectively with a high- (top) and low- (bottom) Alfvén Mach number (M_A) solar wind. (a, d) The speed profile along the streamlines from the simulations (solid). (b, e) The accelerations due to magnetic forces (from the total $\boldsymbol{J} \times \boldsymbol{B}$ force (solid) and from the magnetic pressure gradient force only (dashed)). (c, f) The accelerations due to plasma pressure gradient forces. We observe that most of the acceleration comes from plasma pressure gradient forces in the high M_A case, while most of the acceleration comes from magnetic forces in the low M_A case.

[17] In equation 1, the $\boldsymbol{J} \times \boldsymbol{B}$ term is the total magnetic force, which can be divided into magnetic tension and pressure gradient terms as shown in equation 2. The magnetic tension force (first term on right-hand side (RHS) of equation 2) includes a term that nullifies the parallel (to the magnetic field) component of the magnetic pressure gradient force (second term on RHS), so that the total magnetic force only acts perpendicular to the magnetic field. We have reconstructed in Figure 3 the perpendicular accelerations, resulting from each of the three MHD forces that act along the selected streamlines, as illustrated in equation 3. In addition to parameters defined previously, $\boldsymbol{J}$ is the current density, $\partial \boldsymbol{s}$ is a length element along the streamline, and the three RHS terms of equation 3 are, respectively from left to right, the acceleration due to plasma pressure gradient forces (Figures 3c and 3f), magnetic pressure gradient forces and magnetic tension forces (Figures 3b and 3e). Also, it is known that derivatives are often noisy in numerical calculations [e.g., *Issacson and Keller*, 1966]. Prior to analysis, streamline data have been smoothed (ten-point running average) for sake of cleanliness, but this does not affect the main results.

[18] Figure 3 shows that for the high M_A case (Figures 3a, 3b, and 3c), the magnetic forces are very low and the plasma pressure gradient forces are dominant. The resulting acceleration is gradual so that the magnetosheath flow increases without attaining speeds larger than that of the solar wind itself (for the spatial domain concerned). For the low M_A case (Figures 3d, 3e, and 3f), the magnetic forces are dominant and lead to very strong acceleration up to speeds substantially larger than the solar wind.

[19] In the low M_A case, when integrating the acceleration resulting from each force in the region between -40 R_E to $\sim$20 R_E (i.e., from the maximum of the flows to just inside the bow shock), one finds that the acceleration owing to the magnetic pressure gradient force represents 49% of the total acceleration, while the magnetic tension and plasma pressure gradient accelerations represent 43% and 8%, respectively. These ratios tend to vary as follows: (1) the tension force is more important for streamlines closer to the magnetopause, and (2) the magnetic pressure gradient force is more dominant as one starts the integration of forces further downstream of the shock. The latter is due to the fact that, in the subsolar magnetosheath, the magnetic pressure builds up toward the magnetopause, thus acting against the acceleration. Past the point of maximum magnetic pressure, the magnetic pressure gradient force becomes large and dominant (see Figure 3e). In conclusion, the acceleration due to the magnetic pressure gradient force is globally comparable to that from the magnetic tension force. This acceleration mechanism is not a simple analogy to a slingshot effect [*Chen et al.*, 1993], for which the acceleration ought to be due, at least predominantly, to the magnetic tension force.

[20] We have used idealized steady-state conditions for the purpose of easily identifying and studying individual MHD forces along given streamlines. However, it must be mentioned that non-steady-state and non-ideal-MHD effects, as well as geophysical parameters like the dipole tilt and ionospheric conductivity (e.g., by influencing dayside/lobe reconnection and thus magnetic field pile-up at the dayside), may have important consequences that may for instance explain the difference in flow magnitude between simulations and observations. Such investigation is left for future studies.

5. Conclusion

[21] The present results provide new and unambiguous proof of the occurrence of strong bulk flow accelerations in the near-Earth environment that is demonstrably not the result of magnetic reconnection. The enhanced magnetic forces in the magnetosheath also deform the magnetopause shape, which likely alters the modes of interaction and penetration of the solar wind plasma. The increased velocity shear at the flank magnetopause may help the development of Kelvin-Helmholtz waves, but on the other hand the

enhanced magnetic fields may stabilize the process. Future studies should focus on how this mechanism may affect solar wind plasma entry into the magnetosphere [*Chen et al.*, 1993; *Hasegawa et al.*, 2004].

[22] The driving conditions are a low M_A solar wind and subsequent low-β magnetosheath, which is often typical of CMEs [*Gosling et al.*, 1987; *Lindsay et al.*, 1995; *Farrugia et al.*, 1995]. The effects described here thus condition the magnetosheath-magnetosphere interaction during the passage of such structures at Earth. Under southward IMF, magnetic field pile-up at the dayside magnetopause is lower owing to the occurrence of dayside magnetic reconnection. Yet the entire magnetosheath is characterized by unusually low-β plasma during such solar wind conditions. Thus, although likely weaker under southward, in future studies we will investigate whether these effects may occur during the development of some CME-driven geomagnetic storms.

[23] **Acknowledgments.** The authors are grateful to T. I. Pulkkinen, R. M. Skoug, J. Raeder, and C. Goodrich for comments. We are grateful to the Community Coordinated Modeling Center (CCMC) for the use of models, and to the ACE teams for the use of solar wind data. Work at Los Alamos was performed under the auspices of the US Department of Energy, with support from NASA programs (Guest investigator and Living With a Star TR&T).

References

Cane, H. V., and I. G. Richardson (2003), Interplanetary coronal mass ejections in the near-Earth solar wind during 1996–2002, *J. Geophys. Res.*, *108*(A4), 1156, doi:10.1029/2002JA009817.

Chen, S.-H., M. G. Kivelson, J. T. Gosling, R. J. Walker, and A. J. Lazarus (1993), Anomalous aspects of magnetosheath flow and of the shape and oscillations of the magnetopause during an interval of strongly northward interplanetary magnetic field, *J. Geophys. Res.*, *98*(A4), 5727–5742.

Cowley, S. W. H. (1982), The causes of convection in the Earth's magnetosphere: A review of developments during the IMS, *Rev. Geophys.*, *20*(3), 531–565.

Dungey, J. W. (1961), Interplanetary magnetic field and the auroral zones, *Phys. Rev. Lett.*, *6*, 47–48.

Dunlop, M. W., A. Balogh, and K.-H. Glassmeier (2002), Four-point Cluster application of magnetic field analysis tools: The discontinuity analyzer, *J. Geophys. Res.*, *107*(A11), 1385, doi:10.1029/2001JA005089.

Farrugia, C. J., N. V. Erkaev, H. K. Biernat, and L. F. Burlaga (1995), Anomalous magnetosheath properties during Earth passage of an interplanetary magnetic cloud, *J. Geophys. Res.*, *100*(A10), 19,245–19,257.

Fuselier, S. A., B. J. Anderson, and T. G. Onsager (1997), Electron and ion signatures of field line topology at the low-shear magnetopause, *J. Geophys. Res.*, *102*(A3), 4847–4863.

Gombosi, T. I., et al. (2000), Multiscale MHD simulation of a coronal mass ejection and its interaction with the magnetosphere-ionosphere system, *J. Atmos. Sol. Terr. Phys.*, *62*(16), 1515–1525.

Gosling, J. T., D. N. Baker, S. J. Bame, W. C. Feldman, R. D. Zwickl, and E. J. Smith (1987), Bidirectional solar wind electron heat flux events, *J. Geophys. Res.*, *92*(A8), 8519–8535.

Gosling, J. T., M. F. Thomsen, S. J. Bame, R. C. Elphic, and C. T. Russell (1990a), Plasma flow reversals at the dayside magnetopause and the origin of asymmetric polar cap convection, *J. Geophys. Res.*, *95*(A6), 8073–8084.

Gosling, J. T., M. F. Thomsen, S. J. Bame, T. G. Onsager, and C. T. Russell (1990b), The electron edge of the low latitude boundary layer during accelerated flow events, *Geophys. Res. Lett.*, *17*(11), 1833–1836.

Hasegawa, H., et al. (2004), Rolled-up Kelvin-Helmholtz vortices and associated solar wind entry at Earth's magnetopause, *Nature*, *430*, 755–758.

Howe, H. C., and J. H. Binsack (1972), Explorer 33 and 35 plasma observations of magnetosheath flow, *J. Geophys. Res.*, *77*(19), 3334–3344.

Issacson, E., and H. B. Keller (1966), *Analysis of Numerical Methods*, John Wiley, New York.

Lavraud, B., M. F. Thomsen, B. Lefebvre, S. J. Schwartz, K. Seki, T. D. Phan, Y. L. Wang, A. Fazakerley, H. Rème, and A. Balogh (2006), Evidence for newly closed magnetosheath field lines at the dayside magnetopause under northward IMF, *J. Geophys. Res.*, *111*, A05211, doi:10.1029/2005JA011266.

Lindsay, G. M., C. T. Russell, and J. G. Luhmann (1995), Coronal mass ejection and stream interaction region characteristics and their potential geomagnetic effectiveness, *J. Geophys. Res.*, *100*(A9), 16,999–17,013.

Paschmann, G., et al. (1979), Plasma acceleration at the Earth's magnetopause: Evidence for reconnection, *Nature*, *282*, 243–246.

Petrinec, S. M., T. Mukai, A. Nishida, T. Yamamoto, T. K. Nakamura, and S. Kokubun (1997), Geotail observations of magnetosheath flow near the magnetopause, using Wind as a solar wind monitor, *J. Geophys. Res.*, *102*(A12), 26,943–26,959.

Phan, T.-D., G. Paschmann, W. Baumjohann, N. Sckopke, and H. Lühr (1994), The magnetosheath region adjacent to the dayside magnetopause: AMPTE/IRM observations, *J. Geophys. Res.*, *99*(A1), 121–141.

Ridley, A. J., T. I. Gombosi, and D. L. DeZeeuw (2004), Ionospheric control of the magnetosphere: Conductance, *Ann. Geophys.*, *22*(2), 567–584.

Russell, C. T., and S. M. Petrinec (1996), Comments on "Towards an MHD theory for the standoff distance of Earth's bow shock" by I. H. Cairns and C. L. Grabbe, *Geophys. Res. Lett.*, *23*(3), 309–310.

Siscoe, G. L., et al. (2002), MHD properties of magnetosheath flow, *Planet. Space Sci.*, *50*(5–6), 461–471.

Sonnerup, B. U. O., G. Paschmann, I. Papamastorakis, N. Sckopke, G. Haerendel, S. J. Bame, J. R. Asbridge, J. T. Gosling, and C. T. Russell (1981), Evidence for magnetic field reconnection at the Earth's magnetopause, *J. Geophys. Res.*, *86*(A12), 10,049–10,067.

Spreiter, J. R., A. L. Summers, and A. Y. Alksne (1966a), Hydromagnetic flow around the magnetosphere, *Planet. Space Sci.*, *14*(11), 223–253.

Spreiter, J. R., A. Y. Alksne, and B. Abraham-Shrauner (1966b), Theoretical proton velocity distributions in the flow around the magnetosphere, *Planet. Space Sci.*, *14*(11), 1207–1220.

Zwan, B. J., and R. A. Wolf (1976), Depletion of solar wind plasma near a planetary boundary, *J. Geophys. Res.*, *81*(10), 1636–1648.

J. E. Borovsky, B. Lavraud, E. W. Pogue, and M. F. Thomsen, Space Science and Applications, Los Alamos National Laboratory, P.O. Box 1633, MS D466, Los Alamos, NM 87545, USA. (lavraud@lanl.gov)

A. N. Fazakerley, Mullard Space Science Laboratory, University College London, Holmbury St. Mary, Dorking RH5 6NT, UK.

E. A. Lucek, Blackett Laboratory, Imperial College, Prince Consort Road, London SW7 2BW, UK.

H. Rème, Centre d'Etude Spatiale des Rayonnements, 9 Avenue du Colonel Roche, B.P. 4346, Toulouse F-31000, France.

A. J. Ridley, Center for Space Environment Modeling, University of Michigan, 1416 Space Research Building, 2455 Hayward Street, Ann Arbor, MI 48109-2143, USA.